

PSFC/JA-15-65

Characterization of Density Fluctuations During the Search for an I-mode Regime on the DIII-D Tokamak

**A Marinoni¹, J C Rost¹, M Porkolab¹, A E Hubbard¹, T H Osborne³, A E White¹,
D G Whyte¹, T Rhodes², E M Davis¹, D R Ernst¹,
K H Burrell³ and the DIII-D Team**

¹ Plasma Science & Fusion Center, Massachusetts Institute of Technology, Cambridge, MA 02139-4307, USA

² Department of Physics and Astronomy, University of California, Los Angeles, CA 90095-7099, USA

³ General Atomics, PO Box 85608, San Diego, CA 92186-5608, USA

August 2015

**Plasma Science and Fusion Center
Massachusetts Institute of Technology
Cambridge MA 02139 USA**

This material is based upon work supported by the U.S. Department of Energy, Office of Science under Award Number DE-FG02-94ER54235. Reproduction, translation, publication, use and disposal, in whole or in part, by or for the United States government is permitted.

Characterization of density fluctuations during the search for an I-mode regime on the DIII-D tokamak

A Marinoni¹†, J C Rost¹, M Porkolab¹, A E Hubbard¹, T H Osborne³, A E White¹, D G Whyte¹, T Rhodes², E M Davis¹, D R Ernst¹, K H Burrell³ and the DIII-D Team

¹ Plasma Science & Fusion Center, Massachusetts Institute of Technology, Cambridge, MA 02139-4307, USA

² Department of Physics and Astronomy, University of California, Los Angeles, CA 90095-7099, USA

³ General Atomics, PO Box 85608, San Diego, CA 92186-5608, USA

Abstract. The I-mode regime, routinely observed on the Alcator C-Mod tokamak, is characterized by an edge energy transport barrier without an accompanying particle barrier and with broadband instabilities, known as Weakly Coherent Modes (WCM), believed to regulate particle transport at the edge.

Recent experiments on the DIII-D tokamak exhibit I-mode characteristics in various physical quantities.

These DIII-D plasmas evolve over long periods, lasting several energy confinement times, during which the edge electron temperature slowly evolves towards an H-mode-like profile, while maintaining a typical L-mode edge density profile. During these periods, referred to as I-mode phases, the radial electric field at the edge also gradually reaches values typically observed in H-mode.

Density fluctuations measured with the Phase Contrast Imaging diagnostic during I-mode phases exhibit three features typically observed in H-mode on DIII-D, although they develop progressively with time and without a sharp transition: the intensity of the fluctuations is reduced; the frequency spectrum is broadened and becomes non-monotonic; two dimensional space-time spectra appear to approach those in H-mode, showing phase velocities of density fluctuations at the edge increasing to about 10 km/s. However, in DIII-D there is no clear evidence of the WCM.

Preliminary linear gyro-kinetic simulations are performed in the pedestal region with the GS2 code and its recently upgraded model collision operator that conserves particles, energy and momentum. The increased bootstrap current and flow shear generated by the temperature pedestal are shown to decrease growth rates, thus possibly generating a feedback mechanism that progressively stabilizes fluctuations.

PACS numbers: 52.25.Fi, 52.30.Gz, 52.35.Ra, 52.55.Fa

† Corresponding author: marinoni@mit.edu

1. Introduction

The most common scenario for operation in future fusion reactors is the H-mode regime, which achieves good energy and particle confinement times, higher than in other scenarios, via edge transport barriers in both temperature and density [1]. While it is generally beneficial to fusion reactions to keep the energy confinement as high as possible, it is also desirable to maintain a minimum level of particle transport. Indeed, helium ash from fusion reactions and impurities from plasma-wall interactions must be expelled from the plasma core in order to avoid degrading fusion performance or causing a radiative collapse [2]. In ITER and beyond, it is currently envisioned that the two opposite requirements for energy and particle transport will be fulfilled by adopting the ELMing H-mode regime [3]. This particular H-mode allows the edge to develop gradients in temperature and density steep enough to exceed the peeling ballooning threshold [4, 5] and trigger Edge Localized Modes (ELMs) that, in turn, flush out impurities thus providing a minimum level of particle transport that is required for successful operations. However, ELMs are bursting phenomena that generate large and uncontrolled heat and particle fluxes that are convected directly to the divertor. In ITER, uncontrolled type-I ELMs are expected to convect about 20% of the stored energy in the pedestal region to the divertor target, possibly causing significant cracking, erosion, or even localized melting of the divertor. In general, erosion has to be limited to acceptable levels as the resulting impurity influx would cause major disruptions by radiative collapse which, besides degrading fusion performance, would damage PFCs thus limiting their life [6]. Recent studies suggest that the full tungsten divertor in ITER is expected to suffer melting unless ELMs are controlled in amplitude and/or their footprint is broadened [7]. It is therefore of paramount importance to develop alternative modes of operation that suppress, or properly control, type-I ELMs.

A number of such scenarios are currently being studied by the fusion community and can be essentially cast in three different categories. The first consists of driving non-linearly saturated modes at the edge that, being coupled to the most unstable peeling-ballooning mode, prevent the onset of type-I ELMs; techniques based on this approach are the Quiescent High (QH) mode regime [8] and the Resonant Magnetic Perturbation (RMP) [9]. The second approach is based on triggering ELMs when the pedestal has lower energy than that at the peeling-ballooning limit, so that the resulting heat fluxes are below the damage threshold of PFCs; such techniques, known as ELM pacing, generate small and frequent ELMs and are routinely executed via pellet [10] and gas [11] injection, vertical stabilization control [12], or by means of modulated Electron Cyclotron Heating absorbed near the plasma edge [13]. A third technique aims at developing confinement scenarios that inherently provide necessary energy confinement without the presence of a particle confinement barrier, and thus avoiding the necessity for ELMs for impurity control while simultaneously keeping plasma edge below the peeling-ballooning stability limits. Recent investigations have identified the I-mode regime [14] as a promising candidate which, being the subject of this investigation on the DIII-D

tokamak, is the only method described hereafter.

The I-mode regime, obtained on the Alcator C-Mod tokamak [14] and on the ASDEX-Upgrade tokamak [15], is characterized by three distinct features: edge transport barriers in electron and ion temperature but not in density, a change in the fluctuation characteristics of the pedestal region manifested as a reduction in the intensity of low frequency fluctuations and the appearance of broadband fluctuations known as Weakly Coherent Modes (WCM) [16], and the absence of standard L-H transitions such as a sudden drop in the divertor D_α light or uncontrolled increases in density and/or core radiation. Although energy confinement is better than in L-mode owing to the barrier in temperature, pressure and current gradients at the edge are kept below the peeling-ballooning threshold, resulting in the absence of large ELMs. The WCM are instabilities localized near the temperature pedestal top and are believed to play a similar role to ELMs in ELMing H-modes by regulating particle transport and expelling impurities from the plasma core.

This paper is organized as follows: Section 2 describes how the DIII-D experiments were performed; Section 3 summarizes observations on transport quantities; Section 4 reports on measurements of density fluctuations collected by the Phase Contrast Imaging (PCI) diagnostic; linear gyro-kinetic simulations aimed at interpreting the results are presented in Section 5; conclusions are offered at the end.

2. Experimental set-up

Recent experiments were carried out on the DIII-D tokamak [17] to search for the I-mode regime. In order to explore the operational space required to trigger I-modes, plasma discharges were run spanning a wide parameter space: plasma current I_p in the range 1–1.6 MA, line averaged density $\bar{n}_e = 2\text{--}5 \cdot 10^{19} \text{m}^{-3}$, auxiliary heating power via Neutral Beam Injection (NBI) $P_{\text{NBI}} = 2\text{--}7$ MW, NBI injected torque $T_{\text{NBI}} = 0\text{--}5$ Nm, elongation $\kappa = 1.5\text{--}1.8$, lower triangularity $\delta_l = 0.3\text{--}0.7$ and upper triangularity $\delta_u = 0.3\text{--}0.4$. The toroidal vacuum magnetic field was kept fixed at 2.05 T, resulting in q_{95} between 2.8 and 5. A typical equilibrium used for this I-mode study, along with the physical location of the PCI diagnostic beam, is depicted in Figure 1. Based on experience acquired during I-mode campaigns on the Alcator C-Mod tokamak, plasmas were set in a Lower Single Null (LSN) configuration with the ion ∇B drift pointed away from the primary X-point. This configuration is called “unfavourable direction for the ion ∇B drift” and, being known to significantly increase the amount of external power necessary to trigger the H-mode transition [18, 19], is ideal for I-mode studies as it allows one to execute larger power scans without having the plasma transition into H-mode. The value of the safety factor on axis was generally allowed to decrease below unity as, on the Alcator C-Mod tokamak, sawteeth are generally observed to trigger L-I transitions [14]. The electron temperature was measured by the Thomson Scattering (TS) [20] as well as by the Electron Cyclotron Emission (ECE) diagnostics [21]; density was gauged by TS, CO₂ Interferometer [22] and microwave reflectometry [23]; ion temperature along with

toroidal and poloidal velocities were obtained by the Charge Exchange Recombination diagnostic (CER) [24]; fluctuations were monitored by a number of diagnostics including Beam Emission Spectroscopy (BES) [25], Doppler Back Scattering (DBS) [26] along with the Phase Contrast Imaging (PCI) [27, 28], whose results are the focus of this paper. The normalized radial coordinate used throughout this paper is defined as the squared root of the normalized toroidal flux.

3. Experimental results

Standard L-H transitions are easily identified by a sudden drop in the D_α signal at the divertor and/or by a prompt increase in the line averaged density; other characteristic signatures of the transition are a clear increase in stored energy, normalized β and confinement quality H-factor, as well as a sudden decrease of low frequency turbulent density fluctuations. These are in addition to the defining characteristics of H-mode, such as the formation of clear pedestals in temperature and density radial profiles just inside the separatrix. Since I-mode transitions do not carry any noticeable change in the plasma density, their identification relies on significant increases in temperature gradient at the edge, an increase in stored energy and considerable changes in the edge fluctuations.

As mentioned in Section 2, a large set of parameters was spanned in order to explore accessibility conditions to the I-mode regime on the DIII-D tokamak: heating power was varied in fine steps at various values of density, current, plasma shape and beam torque. It will be shown in the following sections that this scan resulted in a number of cases that show similarities to I-mode plasmas in confinement and equilibrium parameters; however, the WCM, that are a key feature of the I-mode regime as seen on the Alcator C-Mod tokamak [14], have not been detected with any fluctuation diagnostic on DIII-D. As discussed in [29], however, the intensity of the WCM depends on pedestal parameters like q_{95} , T_e and collisionality, and conditions for their excitation are not well understood at the present time. Furthermore, from recent experiments on the Alcator C-Mod tokamak [30] it appears that, at relatively low magnetic field, the I-mode and the H-mode power thresholds are close to each other, preventing the I-mode from fully evolving into a robust regime without transitioning to H-mode; the relatively low magnetic field used to run plasma discharges on DIII-D is therefore likely to set operations in this narrow region. The plasma discharges where we could identify features similar to those characterizing the I-mode regime on the Alcator C-Mod and ASDEX-U tokamaks are, de facto, our I-mode plasmas.

An overview of a typical I-mode discharge can be seen in Figure 2: as the injected power is increased in discrete steps, the stored energy and edge electron temperature increase slowly, at constant D_α light intensity, until the plasma suddenly transitions into H-mode at 3.7 s, when the coupled external power exceeds the H-mode threshold. During the time interval between 2.5 and 3.7 seconds we observe increases in the edge electron temperature and stored energy by a greater percentage than the heating power,

a constant recycling displayed by a steady level of D_α emission indicating that high edge particle transport is maintained [19] and, as will be shown in the next section, a drastic modification of the characteristics of edge fluctuations; for these reasons, in the remainder of the paper, we will refer to this time window as the *I-mode phase*. Note that the I-mode phase bears no relation to the I phase, or intermediate phase, a period of unstable edge transport sometimes observed at the L-H transition [31]. The time evolution of temperature and density profiles shown in Figure 2 is better described by comparing edge radial profiles in L-, I- and H-mode phases. In Figure 3, where such profiles are shown, it is evident how the temperature profile evolves towards a typical H-mode profile with a pedestal like structure at the edge, while the density profile does not show any sign of a pedestal and remains equal to that in L-mode until the H-mode power threshold is reached.

It should be noted, however, that fusion performance in I-mode plasmas obtained in this study is higher than in L-mode but lower than in H-mode plasmas. These reversed ion ∇B drift H-modes achieve electron temperature pedestal heights $T_{e,\text{ped}}$ of about 450-500 eV and confinement quality factors $H_{98,y2}$ of about 1.2, while I-mode phases achieve $T_{e,\text{ped}}$ of about 350 eV and $H_{98,y2}$ of 0.7-0.8, which is still substantially better than in L-mode, whose $H_{98,y2}$ is roughly 0.5. Numerical values of the confinement quality factor are consistent with the T_e profiles in the I-mode phase being in an intermediate state between L- and H-mode.

While the electron temperature at the plasma edge is the best quantity to identify the appearance of the I-mode phase, it is not the only one. The radial electric field (E_r) at the edge also changes compared with profiles obtained during L- and H-mode phases. In Figure 4 we show radial profiles of E_r reconstructed from CER measurements as the plasma transitions through L→I→H-mode phases; we see that the radial electric field steadily and continuously evolves from values usually obtained in L-mode towards those typical of an H-mode plasma, with the diamagnetic component becoming increasingly more important in the region outside the top of the pedestal. The resulting radial shear just inside the separatrix during the I-mode phase is larger than in L-mode plasmas at the same power. A significant E_r well is also observed to develop in I-mode on the Alcator C-mod [32] and ASDEX-U [33] tokamaks. A striking result of this experiment is that the plasma shape, and in particular the triangularity, appears to be one of the key parameters to access the I-mode phase in DIII-D. In Figure 5 we compare the time traces of auxiliary NBI power, stored energy and electron temperature at three radial locations for two plasmas that differ only in the lower triangularity, being equal to 0.5 and 0.7 for discharges #149908 and #149917, respectively. It can be seen how, at 1.5 s, a slight increase in the auxiliary power triggers the I-mode phase, as indicated by the electron temperature at the edge that increases by about 25%. The formation of an E_r well is temporally correlated with the time at which the temperature pedestal forms. The importance of plasma shape as an accessibility conditions for the I-mode regime was also reported by the Alcator C-Mod team [14], and its cause is currently being studied. To conclude, plasmas with characteristics similar to the I-mode regime

observed on the Alcator C-Mod and ASDEX-U tokamaks were obtained on the DIII-D tokamak. Namely, it is possible to identify long phases during which, at the edge, the electron temperature develops a pedestal and the radial electric field forms a well, both of which are among the characteristic signatures of H-mode phases. The density profile, in contrast, remains very close to that in the L-mode part of the discharge and the divertor D_α light is not impacted at all. The I-mode phase can be difficult to identify as, depending on the plasma parameters and on how the heating power is coupled, the transition can be very slow and weak. On the contrary, as it will be shown in the next section, fluctuation measurements from the Phase Contrast Imaging diagnostic can identify the transition in a much sharper way.

4. Measurements of fluctuations

In this paper we will report mainly on fluctuations measurements from the Phase Contrast Imaging (PCI) diagnostic as its wide frequency-wave number response and the fact that it measures the line integral of density fluctuations are advantageous features in experiments characterized by transitions.

The PCI system on DIII-D makes use of a CO_2 laser beam to image the line integral of electron density fluctuations along a vertical chord that is tangent to flux surfaces around mid-radius and at the elevation of the magnetic axis. The location of the vertical chord, depicted in Figure 1, is fixed in space and its value expressed in plasma coordinates obviously depends on the equilibrium. The line integral is imaged onto a linear array of 32 detector elements, allowing the computations of correlation lengths and wave number spectra. The PCI, being a line integrated diagnostic, is only sensitive to fluctuations oriented orthogonally to the direction of propagation of the laser beam and, in the case of negligible electromagnetic fluctuations, orthogonally to equilibrium magnetic field lines. This makes the diagnostic sensitive to wave vectors whose radial and poloidal components vary along the line integral; in particular, the PCI is sensitive to a mixed $(k_\rho-k_\theta)$ everywhere but at the tangency point with any flux surface, i.e. on the mid-plane in DIII-D, where it can only measure k_ρ components.

The difference in density fluctuations between a regular L-mode and an I-mode plasma can be seen by comparing spectra from two discharges with similar parameters, except for a small change in the lower triangularity that allowed one to access the I-mode regime (see Figure 5). In Figure 6 we plot the time evolution of the PCI frequency power spectra, averaged over all the PCI channels, for the two sister discharges of Figure 5. Spectrograms are plotted covering the time interval 0.5-2 s, which is when the two discharges are virtually identical, apart from the value of the lower triangularity. Discharge #149908, i.e. the I-mode plasma, shows a decrease of the intensity of low frequency fluctuations accompanied by an increase in the spectral width at 1.5 s, which is when the edge electron temperature experiences a sudden rise due to a slight augmentation of the auxiliary power (Figure 5). In order to fully appreciate this effect, it has to be noted how the broadening of the spectrum caused by 20% increase

in heating power at 1.5 s is almost one order of magnitude larger than that in the sister discharge #149917; moreover, it is also approximately twice as large as the broadening happening at 1 s, caused by the NBI heating being turned on to deliver 2.24 MW. This abrupt change in the spectral width is a clear indication of an increase of the plasma fluid velocity, and is consistent with the radial electric field reconstruction shown in Figure 4. In order to better illustrate the reduction in the intensity of fluctuations accompanying the frequency broadening of the spectrum, Figure 7 shows frequency power spectra computed in time windows of interest. As the plasma transitions from L- through I- and finally into H-mode, we can observe a progressive reduction of the intensity of fluctuations below 300 kHz. This steady decrease is consistent with a parallel augmentation of the $H_{98,y2}$ confinement enhancement factor reported in Section 3, where we showed a progressive increase in the edge electron temperature gradient and related quantities, including the radial electric field, at constant injected power. Interestingly, the total power of fluctuations during I-mode phases exhibits values that are quantitatively in between those computed during L- and H-mode phases; in the case shown in Figure 7, for example, the total power of fluctuations during the I-mode phase is approximately equal to the arithmetic average of those in L- and H-mode phases.

We can now highlight what is probably the most important feature related to the broadening of the frequency spectrum shown in Figure 7. In addition to the broadening and amplitude reduction, the PCI power spectrum develops a non-monotonic feature in the I-mode phase. Indeed, as soon as the plasma hits the transition, the frequency spectrum develops a local peak above 300 kHz that is reminiscent of that routinely observed in H-mode plasmas. It is important to state that such peaks at high frequency are never observed in regular L-mode plasmas on DIII-D, and that PCI results from dedicated H-mode experiments indicate that they are due to fluctuations localized in the pedestal region, where the radial electric field develops a well [34]. As was mentioned in Section 3, it is not always trivial to identify the I-mode phase due to the gentle nature of its transition that does not show any sharp change in equilibrium quantities, e.g. the divertor D_α light. Based on our current data set, the appearance of the aforementioned peak at high frequency in the PCI spectra coincides with the formation of an electron temperature pedestal, and is therefore a clear signature of a transition into the I-mode phase. This is one of the greatest benefits of monitoring fluctuations with the PCI: the identification of a pedestal in the electron temperature does not necessarily have to rely on accurate radial fits of the edge electron temperature or the electric field which, depending on the quality and quantity of raw data, could prove to be a difficult task. Rather, the edge temperature barrier is identified through an immediately noticeable Doppler shifted PCI spectrum; transitions to I-mode phases are thus efficiently captured by the PCI diagnostic.

Even though the I-mode discharges show notable similarities with I-mode plasmas obtained on the Alcator C-Mod tokamak both in equilibrium parameters and in fluctuations, on DIII-D we do not observe the WCM on any of the fluctuation diagnostics available. In particular, the WCM as observed on the Alcator C-mod tokamak by various

diagnostics, notably the PCI, are characterized by a well defined spatial wave-number and are extended over a broad range of frequencies; instead, the peak at high frequency detected on the PCI spectra at DIII-D extends over a finite region both in frequency and wave-number, which is a typical feature of broadband turbulence. It is an open question whether the WCM are not excited at all or are not visible with the present diagnostic coverage; if the WCM were excited to amplitudes above noise, unless they were always masked by fluctuations generated by broadband turbulence, one would have to postulate that their ballooning character locates them outside of the PCI line of sight, their spatial structure is narrower than the spatial separation of DBS channels and their wavenumber is higher than the BES system response.

Two dimensional frequency-wavenumber spectra extracted from the PCI diagnostic usually carry more complete information about fluctuations, and will be discussed hereafter. The PCI diagnostic measures the line integral of density fluctuations that are Doppler shifted by an amount that depends on the plasma fluid velocity and geometrical factors at the interaction point with the probing laser beam along the line of sight. The resulting two dimensional, frequency-wave number spectrum turns out to be dominated by bands, whose slope is the result of Doppler shifted fluctuations integrated along the laser beam path: at fixed plasma shape, the steeper the slope the higher the Doppler shift. The Doppler shift, in turn, is due to the phase velocity of fluctuations propagating in a plasma that advects at the $E \times B$ velocity. Depending on the velocity magnitude, the shape of the spectrum can be significantly altered: a simple cartoon showing this effect is given in Figure 8 for illustration purposes. The two dimensional spectrum is usually symmetric in wave-number, unless fluctuations as seen from the PCI are not up-down symmetric. Possible causes for such asymmetries are due to the plasma shape being up-down asymmetric or to a substantial shear in the plasma velocity radial profile. Both causes are immediately understandable by realizing that strong asymmetries in plasma shape and strong velocity radial shear alter the orientation, in real space, of fluctuations that mainly propagate in the poloidal direction. Therefore, fluctuations localized below and above the mid-plane and propagating in opposite horizontal directions in real space, would be measured by the PCI as asymmetric in wave-number, even though they had the same wave-numbers in plasma coordinates. While a rather strong geometrical asymmetry is required to see a clear imbalance in the wave-number spectrum, in [34] it is shown how a sheared $E \times B$ velocity in H-mode plasmas can tilt turbulent eddies located below and above the mid-plane in different directions with respect to the probing beam, resulting in an asymmetric spectrum in wave number. This asymmetry is not due to an up-down asymmetry in the strength of the eddies themselves, rather to the transfer function of the PCI diagnostic that mainly measures fluctuations propagating orthogonally to the direction of the probing beam, which on DIII-D is vertical. Our experimental dataset includes triangularity scans that allowed us to exclude plasma shape up-down asymmetries as a possible cause for the afore-mentioned asymmetry in the spectrum.

In Figure 9 we show the time evolution of the phase velocity, obtained as the

ratio of frequency to the wave number that maximizes the power spectrum, averaged over multiple frequencies and corrected for geometrical factors, for fluctuations localized near the edge of the plasma of I-mode discharge #149908. The phase velocity is seen to increase whenever the input power is increased and at 1.5 s, i.e. when the I-mode phase is triggered. It is interesting to note that the phase velocity progressively reaches values typically observed in H-mode, consistent with reconstructions of the radial electric field from the CER diagnostic shown in Section 3. In regular L-H transitions, instead, the phase velocity of fluctuations usually exhibits a sharp discontinuity, displaying much larger values in the H-mode phase. A more striking proof of how fluctuations change between L- and I-mode phases can be seen in Figure 10, where we show two dimensional power spectra of the two sister discharges of Figure 5 in three phases: when they are both in L-mode, when, at same power, #149908 is in the I-mode phase while #149917 remains in L-mode, and when they are both in H-mode. It can be seen that, even though the two discharges are almost identical until 2 s as they differ only in the bottom triangularity, the spectrum computed during the I-mode phase is significantly different from that computed during a regular L-mode phase. Indeed, during the I-mode phase, the spectrum is more asymmetric in wave-number and the phase velocity of fluctuations significantly increases; both of which are characteristics of the H-mode phase. Since the plasma shape is fixed during those three phases, we can conclude that an increasingly sheared $E \times B$ velocity at the edge, as measured by the CER system, tilts fluctuations in such a way as to produce an asymmetric spectrum.

To summarize, the PCI diagnostic measures three distinct features during the I-mode phase: a reduction of the intensity of fluctuations below about 300 kHz, a broadening of the spectrum with the appearance of a peak at high frequency that is reminiscent of what is commonly observed during H-mode phases, and an increase of the phase velocity of fluctuations towards values typically measured in H-mode. It is important to note two key characteristics of these three features: firstly, all of them happen simultaneously; secondly, they become progressively more evident with time, consistent with the time evolution of transport parameters shown in Section 3.

Even though the I-mode phase in DIII-D does not, in general, show confinement properties as good as in H-mode, it does show fluctuation characteristics that are reminiscent of H-mode phases, but without ELMs. Therefore, since it is challenging to efficiently diagnose and study the dynamics of regular L-H transitions due to its extremely fast evolution, the long duration of the I-mode phase makes it also an ideal test-bed to study the H-mode triggering mechanism.

5. Gyrokinetic modeling

Simulations were performed with the gyrokinetic (GK) flux-tube GS2 code [35] that solves the GK Vlasov–Maxwell system of equations as an initial value problem. The gyrokinetic GYRO code [36], run both as an initial value and as an eigenvalue solver, and the gyro-fluid TGLF code [37] were used to benchmark the results from GS2. In view

of the limited knowledge about the plasma edge from the gyrokinetic standpoint, the modeling work presented in this paper is limited to exploratory local linear simulations for which the gyrokinetic ordering is valid, we found reasonable agreement among the afore-mentioned codes and understandable dependences of the solution on plasma parameters. A much more rigorous validation of gyrokinetic modelling near the plasma edge will have to rely on numerical tools specifically developed to handle the plasma region across the separatrix, as well as on experimental benchmarks.

Particle drifts and geometric coefficients are computed in real geometry: an initial equilibrium reconstruction was performed by the EFIT code [38] constrained by measurements from magnetic loops and the Motional Stark Effect (MSE) diagnostic [39]; the 1.5 dimensional ONETWO transport code [40] was used to derive the steady-state current profile, which was then provided as input to the EFIT code during the calculation of the complete kinetic equilibrium, which is subsequently read directly by GS2 and GYRO. This method ensures a correct evaluation of the magnetic geometry.

Convergence studies performed during this modelling indicate that the fluctuating parallel vector potential must be included in the calculations, while retaining the fluctuating component of the parallel magnetic field does not significantly alter the results. Two kinetic species were retained, with impurities only contributing to the effective charge value used to compute the collision frequency; the inclusion of one impurity as a kinetic species does not significantly alter the results. The poloidal wave vectors shown below have zero radial component, which were always found to be the most unstable mode. Simulations benchmarked against GYRO were in the collisionless regime, while collisional simulations were computed only with the GS2 code, as it implements a recently developed collisional operator that conserves particles, energy and momentum [41]. The need of this advanced collision operator was dictated by the high values of collisionality ν^* that, at the top of the pedestal, are greater than one.

Various flux surfaces near the plasma edge were examined, from the outer part of the temperature pedestal to inner regions well inside it. Results shown in this section refer to $\rho = 0.945$, i.e. in the pedestal, and $\rho = 0.8$ which, being away from the steep gradient region, constitutes a reference location for mode comparison. The choice of the flux surface located at $\rho = 0.945$ was dictated by practical reasons that emerged when comparing L-mode and I-mode phases: it is in a narrow region near this flux surface that the Doppler Back Scattering diagnostic detects the largest decrease in the intensity of fluctuations (see Figure 11), and that the reconstructed E_r radial profile is expected to generate a frequency Doppler up-shift measured by the PCI diagnostic that is consistent with experimental two dimensional (f-k) spectra. This radial location, which is also where the pressure radial gradient reaches its maximum, is then assumed to be the dominant source of fluctuations measured by the PCI diagnostic that are used to compare L- and I-mode phases.

To verify the results and to assess the impact of experimental uncertainties, we performed sensitivity scans by varying density and temperature profiles within error bars. The minor changes to real frequencies and to the envelope of eigenfunctions

resulting from these variations indicate that the experimental parameters are not close to any threshold. Uncertainty tests can also be used as an indication of the main instability drive by monitoring how growth rates, γ , respond to varying parameters. When modifying a given physical quantity X by a few percent of its value, the resulting relative variation $\delta \ln(\gamma)/\delta \ln(X)$ is found to be greater than unity only for the electron temperature scale length, which is then assumed to be the dominant driving energy. Increasing T_e/T_i , R/L_{n_e} and R/L_{T_i} are found to be stabilizing. Increasing collisionality is also stabilizing, which rules out the Dissipative Trapped Electron Modes (DTEM) as a significant instability in this regime. We note that complex frequencies of the modes are strongly impacted when β exceeds twice the experimental value.

In Figure 12 we summarize differences in the character of the instability between the two radial locations considered during the I-mode phase. At the inner location, away from the steep gradient region, the spectrum is characterized by an ITG mode and an TEM mode at lower and higher wave-numbers, respectively, with well defined phase velocities. The envelope of the field potentials along the field line is very regular and peaked at the outboard mid-plane, and is consistent with numerous results already published in the literature. At the outer location, i.e. $\rho = 0.945$, there are still two distinct branches at lower and higher wave-numbers, but with notable differences with respect to those at the inner location. Firstly, for $k_\theta \rho_i < 1$, as the wave-number increases the dominant instability reverses its direction of propagation from the electron to the ion diamagnetic direction, with growth rates peaking at zero phase velocity in the plasma frame, which is reminiscent of a particular class of trapped particle instabilities called the ubiquitous mode [42]. Secondly, for $k_\theta \rho_i > 1.5$, the group velocity of the electron mode is approximately null (see Figure 12b). Thirdly, field potentials along the field line are reasonably smooth for wave-vectors lower than that at which the phase velocity goes through zero, while they develop off-axis peaks at all higher wave-numbers. Similar characteristics were found by other authors as well, even though in different regimes [43, 44]. The fluctuating distribution function, which usually shows signatures of the dominant instability in phase space, e.g. a clear peak in the trapped region for resonating TEM modes, does not clearly identify the aforementioned modes as TEM because the imbalance between the trapped and the untrapped region is not always significant. Therefore, also due to the irregular character of complex frequencies and field potentials along the field line, it is difficult to describe the turbulent edge of these plasmas with a model that considers the entire spectrum to be dominated by only one instability. Another feature that distinguishes the low wave-number modes at the outer location from regular ITG or TEM turbulence is the cross phase between density and temperature fluctuations $\theta_{n,T}$. While, at the inner location, the ion and the electron modes show, respectively, finite positive and negative phase shifts that agree with theoretical expectations based on ITG and TEM turbulence [45], the ubiquitous-like mode at the outer location displays a near zero phase shift, with a negligible dependence on collisionality. In case the plasma edge is sufficiently optically thick, $\theta_{n,T}$ can be directly measured and may provide a valid experimental benchmark.

Based on mixing-length arguments, transport coefficients can be roughly estimated by $\chi = \gamma / \langle k_{\perp}^2 \rangle$ [46], where an effective k_{\perp} can be computed as a field line average weighted by the field potentials [47]. Therefore, even though the growth rates of electron modes at $k_{\theta}\rho_i > 1$ increase steadily, instabilities at those high wave-numbers are not expected to cause significant transport[†]. It is interesting to compare complex frequencies at the very edge, i.e. $\rho = 0.945$, between experimental profiles measured during regular L-mode and I-mode phases. Larger gradients in the temperature radial profile during the I-mode phase slightly enhance growth rates in physical units that, for $k_{\theta}\rho_i \leq 1$, do not exceed $250 \cdot 10^3$ rad/s. Cross phases between temperature and density fluctuations with the field potentials are not significantly altered by the transition, which results in a slight increase of the estimated mixing length transport when the plasma transitions from L- to I-mode phases. This, being in contradiction with the clear increase in confinement at constant auxiliary power and the reduction in the intensity of fluctuations measured by the PCI diagnostic, requires additional physical effects in the model, e.g. flow shear and non-linear effects. Discarding non-linear effects that are not included in this modelling work, we now turn to analyze the well known stabilizing effect exerted by flow shear on ion scale fluctuations [48]. As shown in Section 3, since I-mode plasmas develop a significantly larger E_r than L-mode plasmas in the pedestal region, it is natural to compare the increasingly larger flow shear to growth rates as the plasma evolves from L- to I-mode. At $\rho = 0.945$, the Hahm-Burrell shearing rate [49] during L- and I- phases is in the range $200\text{--}350 \cdot 10^3$ rad/s and $400\text{--}600 \cdot 10^3$ rad/s, respectively, depending on how radial fits are computed and including uncertainties. Turbulence quenching is expected to take place when the shearing rate γ_E and the maximum linear growth rate in the absence of flow shear γ_{\max} satisfy the relation $\alpha_E \gamma_E \simeq \gamma_{\max}$, where α_E is a numerical coefficient that, based on a fit on non-linear gyrokinetic simulations of ITG-TEM turbulence at mid-radius, can be estimated to about 0.4 for the plasma shape adopted in these experiments [50]. Therefore one could expect that, as the pressure profile develops a pedestal at the edge, the increasingly larger shearing rate would overcome the growth rate of the most unstable mode, thus progressively stabilizing fluctuations, in agreement with the measurements[‡]. Transport coefficients would then be reduced leading, at constant injected power, to a local increase of the temperature gradient that, in turn, would enhance the flow shear thus providing a stabilizing feedback loop. This reasoning, however, has to be quantitatively verified by non-linear gyrokinetic simulations valid in the pedestal region as the widely used rule of thumb of visually comparing the Hahm-Burrell shearing rate to the linear growth rates of the most unstable mode may not hold up in this context.

Another mechanism that may play a role in these experiments is the following: as the pressure profile develops a pedestal at the edge, the increasingly larger bootstrap

[†] unless in the presence of inverse cascade events, which cannot be predicted by linear simulations and are thus excluded from the discussion

[‡] A similar conclusion is reached by considering the flux surface constant Waltz-Miller formula [51] for the flow shear and the relative numerical fit for the coefficient

current modifies the equilibrium and flattens the radial profile of the safety factor; this alters particle drifts and results in a modifications of real frequencies and growth rates. In order to test this effect, we performed simulations of one of our I-mode discharge at the usual edge location in the temperature pedestal, i.e. $\rho = 0.945$, for a regular and a kinetic equilibrium. The density and temperature profiles are kept fixed, resulting in the two simulations being identical in everything but in the equilibrium, with a reduction of 11% in the magnetic shear caused by the bootstrap current at $\rho = 0.945$. In Figure 13, where we compare real frequencies and growth rates, we can observe how, using a kinetic equilibrium, growth rates decrease by about 8% with respect to the regular equilibrium, thus proving a direct impact of the bootstrap current on the mode stability. It has to be stressed that the reduction in the growth rates, even though it might not appear to be significant, is actually comparable to the reduction in the intensity of fluctuations measured by the PCI which, depending on discharge and time instant considered, is in the range 10–20%. This result suggests an explanation for the experimental observations reported in Section 3 and 4 that is complementary, although similar, to the effect exerted by flow shear. If, under certain experimental conditions, such as for specific values of collisionality or plasma shape, it was possible to drive current near the edge of the plasma, the resulting modification to the equilibrium would start reducing the intensity of fluctuations. Transport coefficients would then be reduced leading, at constant injected power, to a local increase of the temperature gradient that, in turn, would drive more current thus providing a stabilizing feedback loop. Both mechanisms are consistent with a progressive stabilization of the intensity of fluctuations measured by the PCI diagnostic, as well as with a steady increase of the temperature gradient and of the radial electric field measured by other diagnostics. Non-linear simulations are now required to compare the relative impact of the two aforementioned stabilizing loops and, most importantly, whichever mechanism turns out to have the major effect in quenching fluctuations, it should only affect energy transport as I-mode plasmas are characterized by an L-mode particle transport.

6. Summary and Conclusions

Recent experiments were carried out on the DIII-D tokamak to search for the I-mode regime which, featuring good energy confinement properties without large type-I ELMs, may be an attractive candidate for operations in ITER and beyond. Selected discharges show notable similarities with I-mode plasmas in confinement and equilibrium parameters, while fluctuations measured by the Phase Contrast Imaging diagnostic (PCI) show characteristics typically observed during DIII-D H-mode phases. More specifically, these plasmas evolve over long periods, lasting several energy confinement times, during which the edge electron temperature evolves towards a pedestal-like profile 0.35 keV high. During these transient phases, referred to as I-mode phases, plasmas maintain a typical L-mode edge density profile. The radial electric field at the edge also progressively reaches values typically observed in H-mode. It is important to note

that, unlike the H-mode transition, the I-mode phase is not characterized by abrupt changes in equilibrium quantities, such as a sudden drop in the divertor D_α light, which makes the identification of the transition more difficult. During the I-mode phase, fluctuations measured by the PCI diagnostic show three distinct features typical of H-mode spectra: a reduction of the intensity of fluctuations below about 300 kHz, a broadening of the frequency spectrum with the appearance of a peak at high frequency that is never observed in L-mode, and an increase of the phase velocities towards values typically measured in H-mode. All these features are immediately observable from the PCI data which, as opposed to diagnostics monitoring equilibrium quantities, captures very efficiently the transition.

In I-mode plasmas on Alcator C-Mod, it is believed that broadband instabilities, known as Weakly Coherent Modes (WCM), regulate particle transport to levels typically observed in L-mode. In DIII-D we do not observe any evidence of such modes in any of the fluctuation diagnostics, notably on PCI. However, I-mode plasmas on DIII-D, Alcator C-Mod and ASDEX-U show notable differences in the pedestal parameters believed to regulate the intensity of the WCM. Future work on DIII-D will explore the dependence of confinement factor on magnetic field intensity, geometry and type of heating in these I-mode phases.

Preliminary linear gyro-kinetic simulations at the edge show the existence of electron modes driven unstable by R/L_{Te} and having field potentials with peaks in amplitude located away from the outboard mid-plane. Increased bootstrap current and flow shear generated by the temperature pedestal progressively reduce growth rates, the intensity of fluctuations and the associated anomalous transport. At fixed auxiliary power, this would translate in a further steepening of the temperature gradient which, in turn, would drive more bootstrap current and increase flow shear. This results in a stabilizing feedback mechanism which is consistent with the progressive stabilization of fluctuations observed with the PCI diagnostic and the steady increase in the edge electron temperature gradient. Detailed non-linear simulations with validated gyrokinetic codes will be necessary to determine if such speculative postulates would explain the transition to I-mode and/or H-mode plasmas.

Acknowledgements

This material is based upon work supported by the U.S. Department of Energy, Office of Science under Award Number DE-FG02-94ER54235. The authors would like to thank Drs. J. Candy, G. Staebler, F. Ryter, L. Zeng and Y. Zheng for helpful discussions, and the authors of the GS2 code for releasing the source.

References

- [1] Loarte A *et al.* 2007 *Phys. Scr.* **T128** 222
- [2] Stacey W M 1997 *Phys. Plasmas* **4** 1069

- [3] Shimada M *et al.* 2007 *Nucl Fusion* **47** S1 *Progress in the ITER Physics Basis Chapter 1: Overview and summary*
- [4] Hegna C C *et al.* 1996 *Phys. Plasmas* **3** 584
- [5] Connor J W *et al.* 1998 *Phys. Plasmas* **5** 2687
- [6] Loarte A *et al.* 2007 *Nucl Fusion* **47** S03 *Progress in the ITER Physics Basis Chapter 4: Power and particle control*
- [7] Pitts R A *et al.* 2013 *Bull. Am. Phys. Soc.* **58**
- [8] Greenfield C M *et al.* 2001 *Phys. Rev. Lett.* **86** 4544
- [9] Lang P T *et al.* 2013 *Nucl. Fusion* **53** 043004
- [10] Lang P T *et al.* 2004 *Nucl. Fusion* **44** 665
- [11] Lennholm M *et al.* 2015 *Nucl. Fusion* **55** 063004
- [12] de la Luna E *et al.* Proc. 24th IAEA Fusion Energy Conf., San Diego, CA, (USA) 2012 *The effect of ELM pacing via vertical kicks on the access to stationary H-mode with good confinement (H98 1) on JET*
- [13] Felici F *et al.* 2013 *Nucl. Fusion* **53** 113018
- [14] Whyte D G *et al.* 2010 *Nucl. Fusion* **50** 105005
- [15] Ryter F *et al.* 38th EPS, Strasbourg (F) 2011 *I-mode studies at ASDEX Upgrade*
- [16] Dominguez A 2012 *Study of density fluctuations and particle transport at the edge of I-mode plasmas* Ph.D. thesis Massachusetts Institute of Technology
- [17] Luxon J L 2002 *Nucl. Fusion* **42** 614
- [18] Hubbard A E *et al.* 2007 *Phys. Plasmas* **14** 056109
- [19] Team A 1989 *Nucl. Fusion* **29** 1959
- [20] Ponce-Marquez D M *et al.* 2010 *Rev. Sci. Instrum.* **81** 10D525
- [21] Austin M E and Lohr J 2003 *Rev. Sci. Instrum.* **74**
- [22] Zeeland M A V *et al.* 2006 *Rev. Sci. Instrum.* **77** 10F325
- [23] Zeng L *et al.* 2001 *Rev. Sci. Instrum.* **72**
- [24] Seraydarian R P and Burrell K H 1986 *Rev. Sci. Instrum.* **57**
- [25] McKee G *et al.* 1999 *Rev. Sci. Instrum.* **70**
- [26] Peebles W A *et al.* 2010 *Rev. Sci. Instrum.* **81** 10D902
- [27] Coda S *et al.* 1992 *Rev. Sci. Instrum.* **63** 4974
- [28] Dorris J R *et al.* 2009 *Rev. Sci. Instrum.* **80** 023503
- [29] Hubbard A E *et al.* 2011 *Phys. Plasmas* **18** 056115
- [30] Hubbard A E *et al.* paper presented at the 25th IAEA Fusion Energy Conference, St. Petersburg (Ru) 2014 *Multi-device Studies of Pedestal Physics and Confinement in the I-mode Regime, 6/612*
- [31] Colchin R J *et al.* 2002 *prl* **88**(25) 255002
- [32] Theiler C *et al.* 2014 *Nucl. Fusion* **54** 083017
- [33] Manz P *et al.* US/EU Transport Task Force Workshop, Salem, MA (USA) 2015 *Geodesic oscillations and the weakly coherent mode in I-mode in ASDEX Upgrade*
- [34] Rost J C *et al.* 2014 *Phys. Plasmas* **21** 062306
- [35] Kotschenreuther M *et al.* 1995 *Comput. Phys. Comm.* **88** 128
- [36] Candy J and Waltz R E 2003 *J. Comput. Phys.* **186** 545
- [37] Staebler G M *et al.* 2005 *Phys. Plasmas* **12** 102508
- [38] Lao L L *et al.* 1985 *Nucl. Fusion* **25** 1611
- [39] Wróblewski D *et al.* 1990 *Rev. Sci. Instrum.* **61** 3552
- [40] Pfeiffer W W *et al.* 1980 Onetwo: A computer code for modeling plasma transport in tokamaks Tech. Rep. GA-A16178 General Atomics
- [41] Barnes M *et al.* 2009 *Phys. Plasmas* **16** 072107
- [42] Coppi B and Pegoraro F 1977 *Nucl. Fusion* **17** 969
- [43] Hatch D *et al.* 2015 *Nucl. Fusion* **55** 063028
- [44] Ernst D R *et al.* 2009 *Phys. Plasmas* **16** 055906

- [45] Staebler G M private communication
- [46] Kadomtsev B B 1965 *Plasma turbulence* (Academic Press LONDON AND NEW YORK)
- [47] Marinoni A *et al.* 2009 *Plasma Phys. Control. Fusion* **51** 055016
- [48] Terry P W 2000 *Rev. Mod. Phys.* **72**(1) 109–165
- [49] Burrell K H 1997 *Phys. Plasmas* **4** 1499
- [50] Kinsey J E *et al.* 2007 *Phys. Plasmas* **14** 102306
- [51] Waltz R E and Miller R L 1999 *Phys. Plasmas* **6** 4265

Figure captions

Figure 1. Schematic view of the DIII-D poloidal cross section. Flux surfaces of one of the actual lower single null plasmas used in the experiments are represented in red, the PCI beam path in purple. Plasma current and toroidal magnetic field are oriented in the counter clock-wise direction as seen from the top, resulting in the $B \times \nabla B$ drift to be directed away from the X point

Figure 2. Overview of DIII-D discharge #155503, one of the I-mode plasmas. Time history of (left axis, solid blue line) plasma current, divertor D_α , neutral beam power, line averaged electron density and (right, dashed green line) internal inductance, radiated power, stored energy, edge electron temperature. The yellowed region indicates the I-mode phase interval between 2.5 and 3.7 seconds.

Figure 3. Radial profiles in the outer part of the normalized minor radius for electron temperature (a) and density (b) during L-mode (blue stars), I-mode (green diamonds) and H-mode (red squares) phases of discharge #155503. Relative uncertainties are within 5% inside $\rho = 0.9$ and within 10% for $0.9 < \rho < 1$, as measured by the TS system.

Figure 4. Radial electric field, plotted as a function of the major radius minus the radial position of the separatrix, reconstructed from the force balance equation. The radial shear during the I-mode phase of discharge #149908 (a) is larger than in L-mode at the same power, as indicated by a regular L-H transition in sister discharge #149917 (b). In the time window 0-2 s the two plasmas only differ in the lower triangularity.

Figure 5. Time evolution of auxiliary NBI power, stored energy and electron temperature at three radial locations for similar discharges #149908 (I-mode, green dash-dotted), and #149917 (regular L-mode, blue solid) that differ only in the lower triangularity in the shown time window. The transition into the I-mode phase happens at 1.5 s, when the injected time averaged power is increased from 2.24 MW to 2.72 MW.

Figure 6. Auxiliary power (top) and power spectrogram from PCI (bottom), in logarithmic scale and arbitrary units, for I-mode discharge #149908 (left) and regular L-mode sister discharge #149917 (right). Density fluctuations are approximately equal until 1.5 s, when discharge #149908 transitions into the I-mode phase, showing a robust increase in bandwidth for a modest increase in input power.

Figure 7. Power spectra of density fluctuations measured by the PCI diagnostic on the I-mode discharge #153031 during L-mode (blue), I-mode (green) and H-mode (red) phases. Compared to L-mode, during I- and H-mode phases the intensity of fluc-

tuations is progressively reduced and spectra develop a peak at high frequency.

Figure 8. Schematic representation of a typical two dimensional, frequency-wave number, spectrum obtained from the Phase Contrast diagnostic. The line integral generates bands that are approximately symmetric in wave-number for up-down symmetric plasmas. An increased fluid velocity differentially shifts up in frequency fluctuations at different wave-numbers according to the relation $\Delta\omega = \mathbf{k} \cdot \mathbf{v}$, thus increasing the overall group velocity.

Figure 9. Time evolution of auxiliary beam power (a) and phase velocities of fluctuations at the edge reconstructed from the PCI diagnostic (b) for I-mode discharge #149908. The phase velocity shows breaks in slope at the transition into the I-mode phase at 1.5 s and whenever the beam power is increased; it eventually reaches values obtained in H-mode.

Figure 10. Comparison of the time evolution of two dimensional, frequency-wave number, power spectra of density fluctuations for sister discharges #149908 (a-b-c) and #149917 (d-e-f). While the spectra are similar in the early phase of the discharge (a vs. d), the I-mode phase (b) features the characteristics of an H-mode phase (c); namely, the spectrum becomes more asymmetric in wave number and the phase velocity significantly increases. The two spectra during H-mode are not directly comparable to each other as the two discharges were heated differently after 2 s.

Figure 11. From top to bottom, time evolution of divertor D_α light, line averaged electron density from CO_2 interferometer, and rms signal of the Doppler Back-Scattering diagnostic for discharge #155503. Channels in the region $0.9 \leq \rho \leq 0.95$ detect the most significant decrease of the intensity of fluctuations in the I-mode time window 2.5-3.7 s.

Figure 12. Real frequency and growth rates as a function of wave-number (top), electrostatic (middle) and parallel vector potentials (bottom) as a function of the ballooning angle computed at two radial locations: $\rho = 0.8$ (a-c-e, left) and $\rho = 0.945$ (b-d-f, right) for I-mode discharge #155503. The sign convention is such that positive real frequencies are in the ion diamagnetic direction. The electron to ion temperature ratio is equal to about 0.7 at both radial locations.

Figure 13. Real frequency (a, left) and growth rates (b, right) as a function of wave-number computed in the middle of the electron temperature pedestal for I-mode discharge #155503 at $\rho = 0.945$. Simulations differ only in the equilibrium; the bootstrap current lowers the magnetic shear by 11% and reduces growth rates.

List of figures

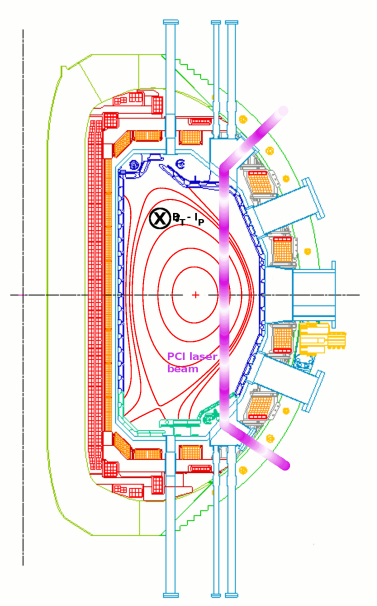


Figure 1.

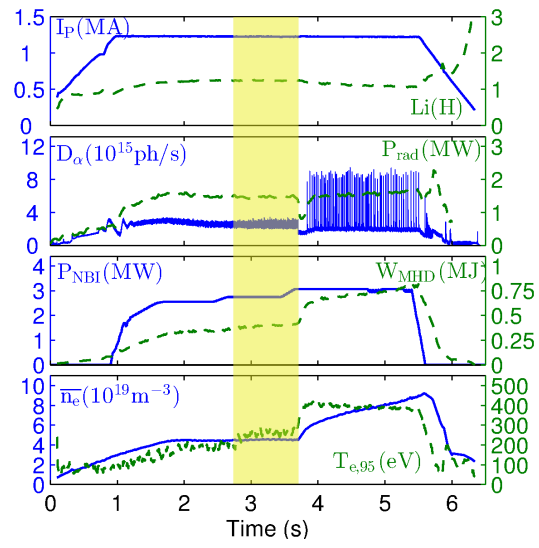


Figure 2.

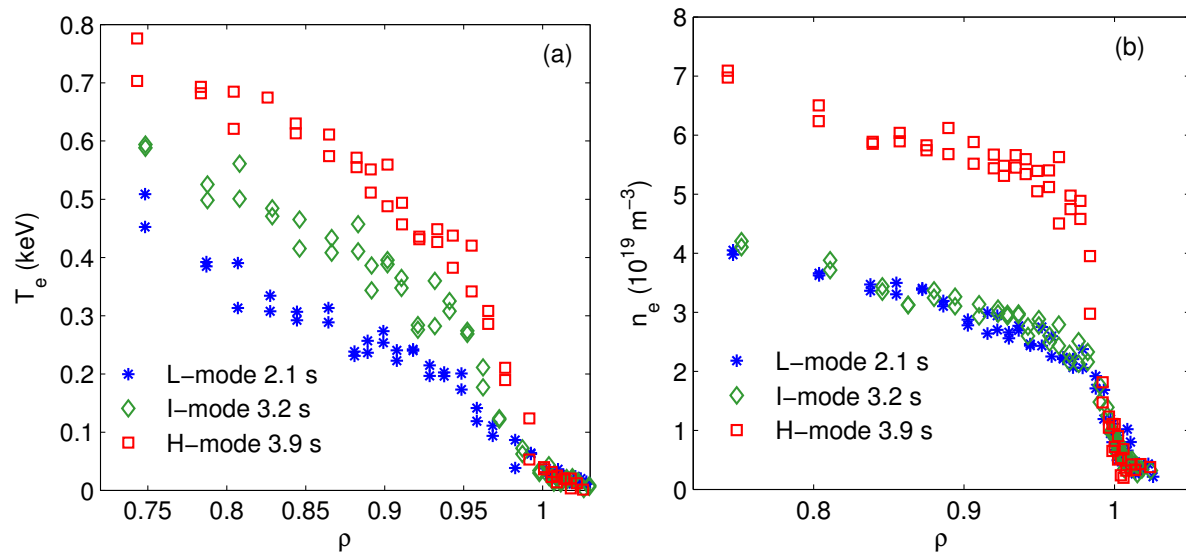


Figure 3.

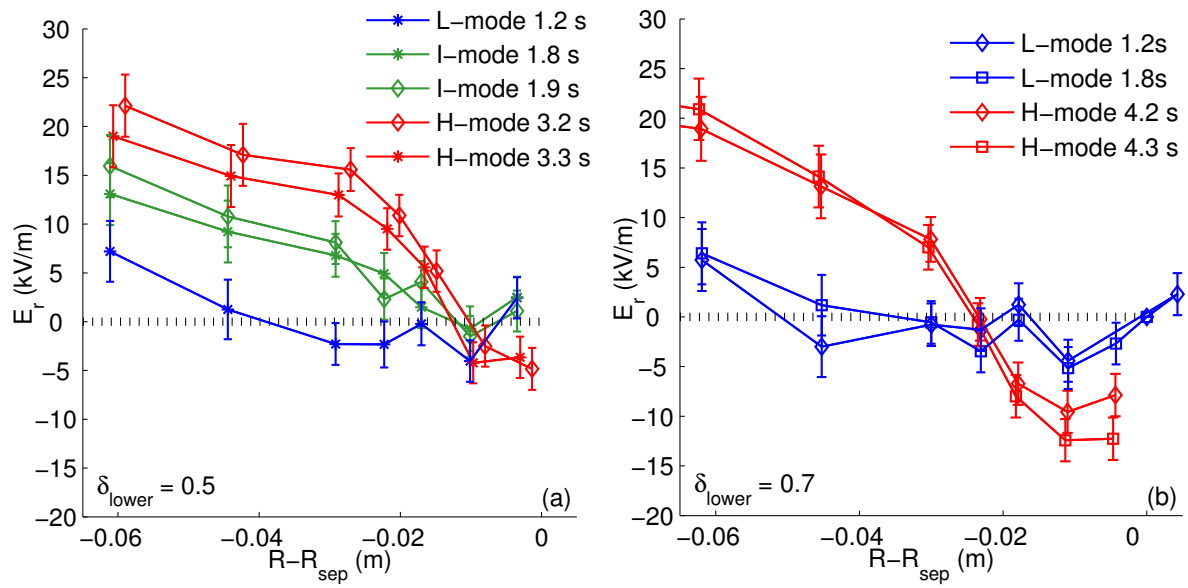


Figure 4.

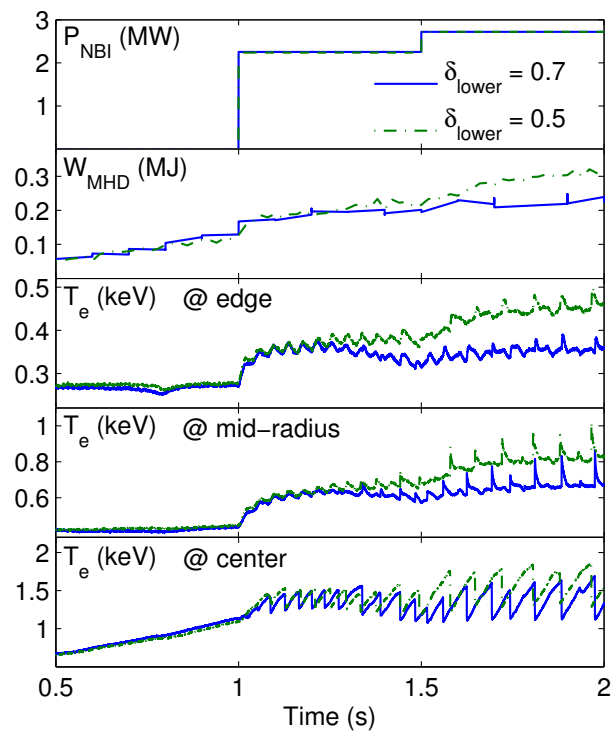


Figure 5.

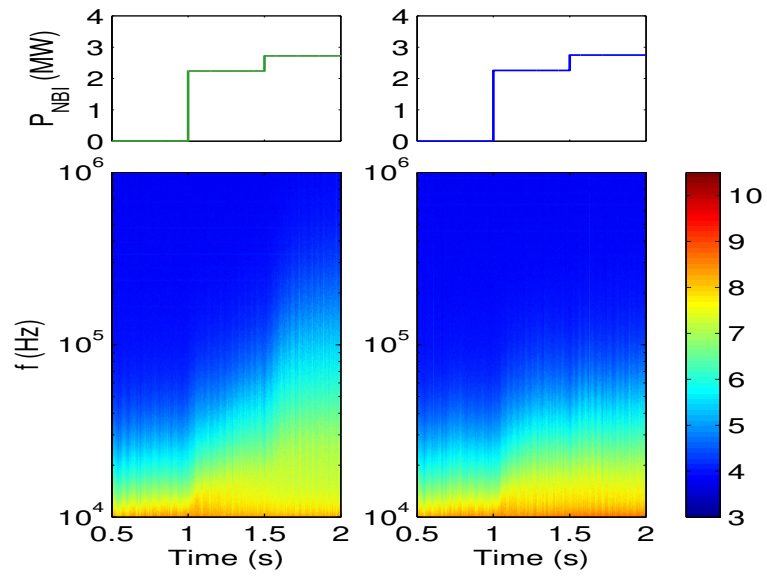


Figure 6.

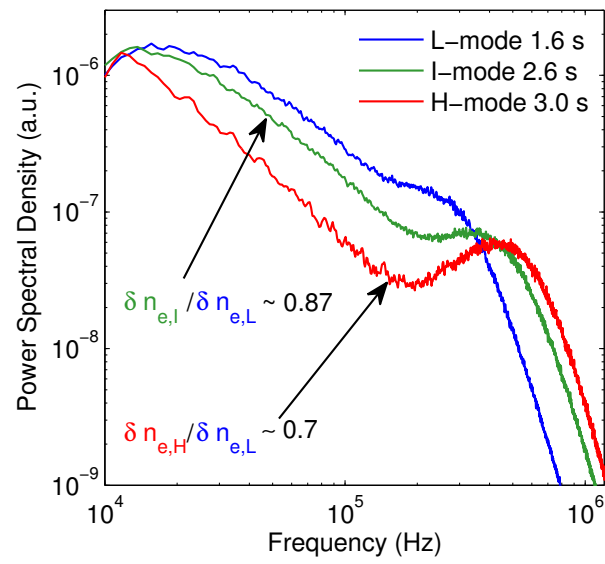


Figure 7.

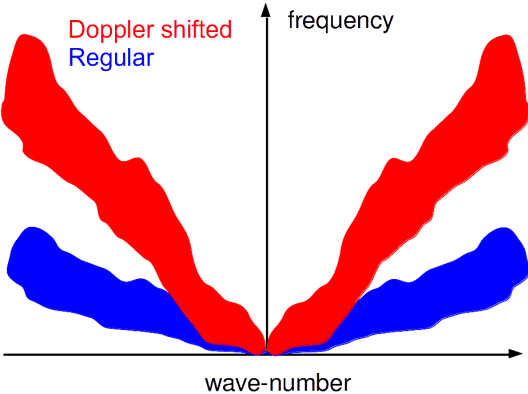


Figure 8.

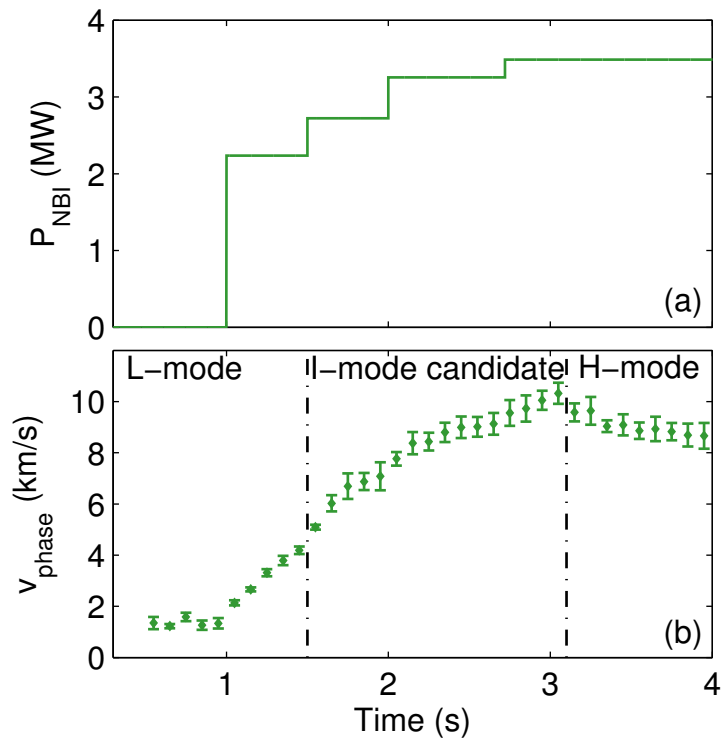


Figure 9.

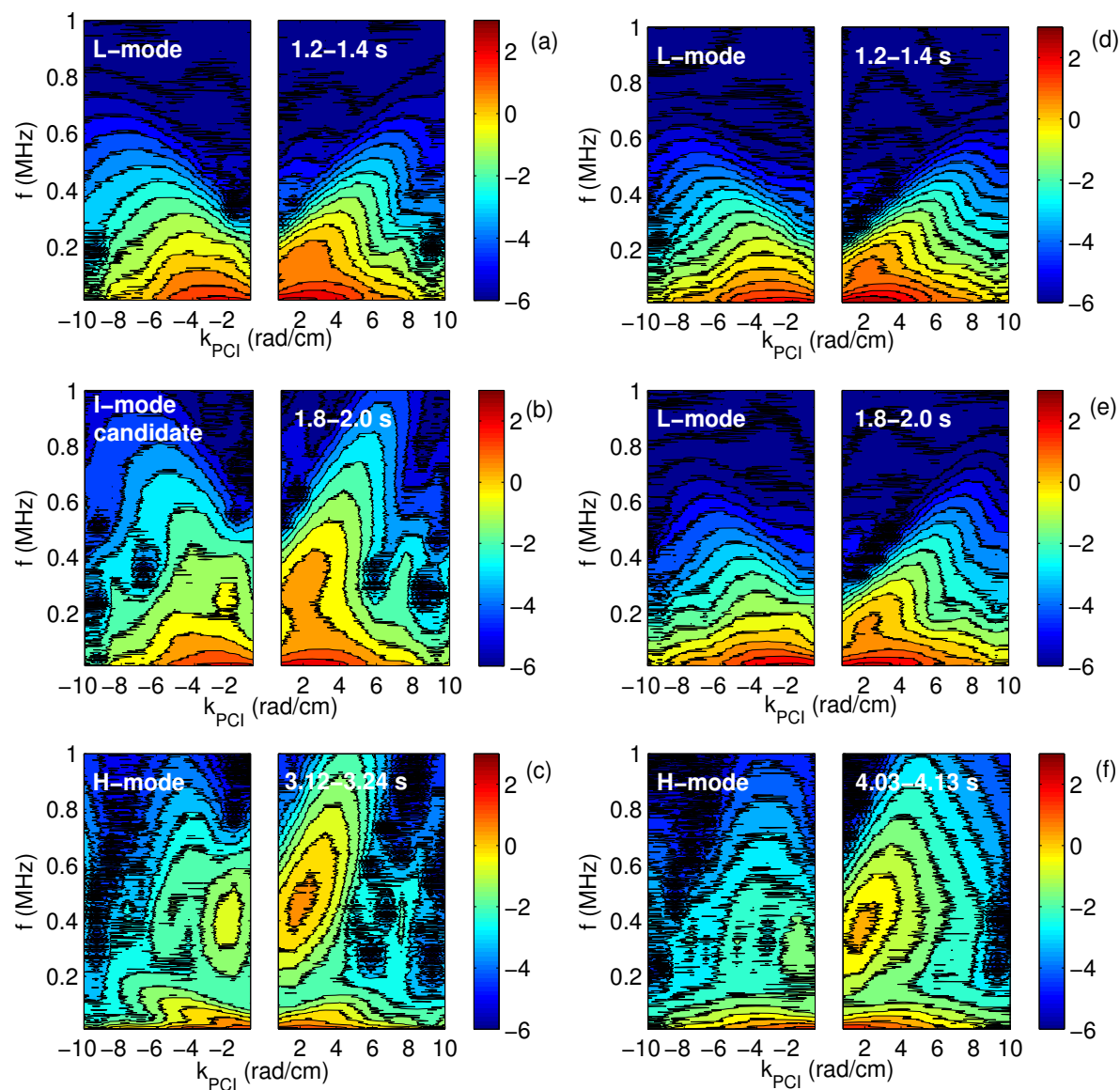


Figure 10.

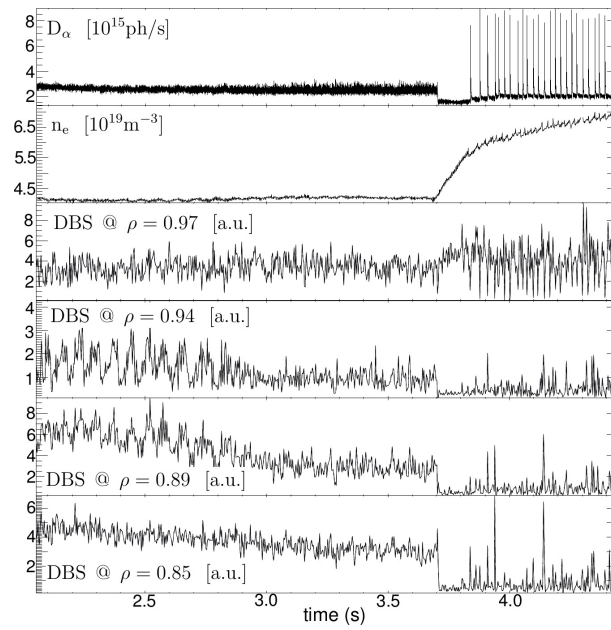


Figure 11.

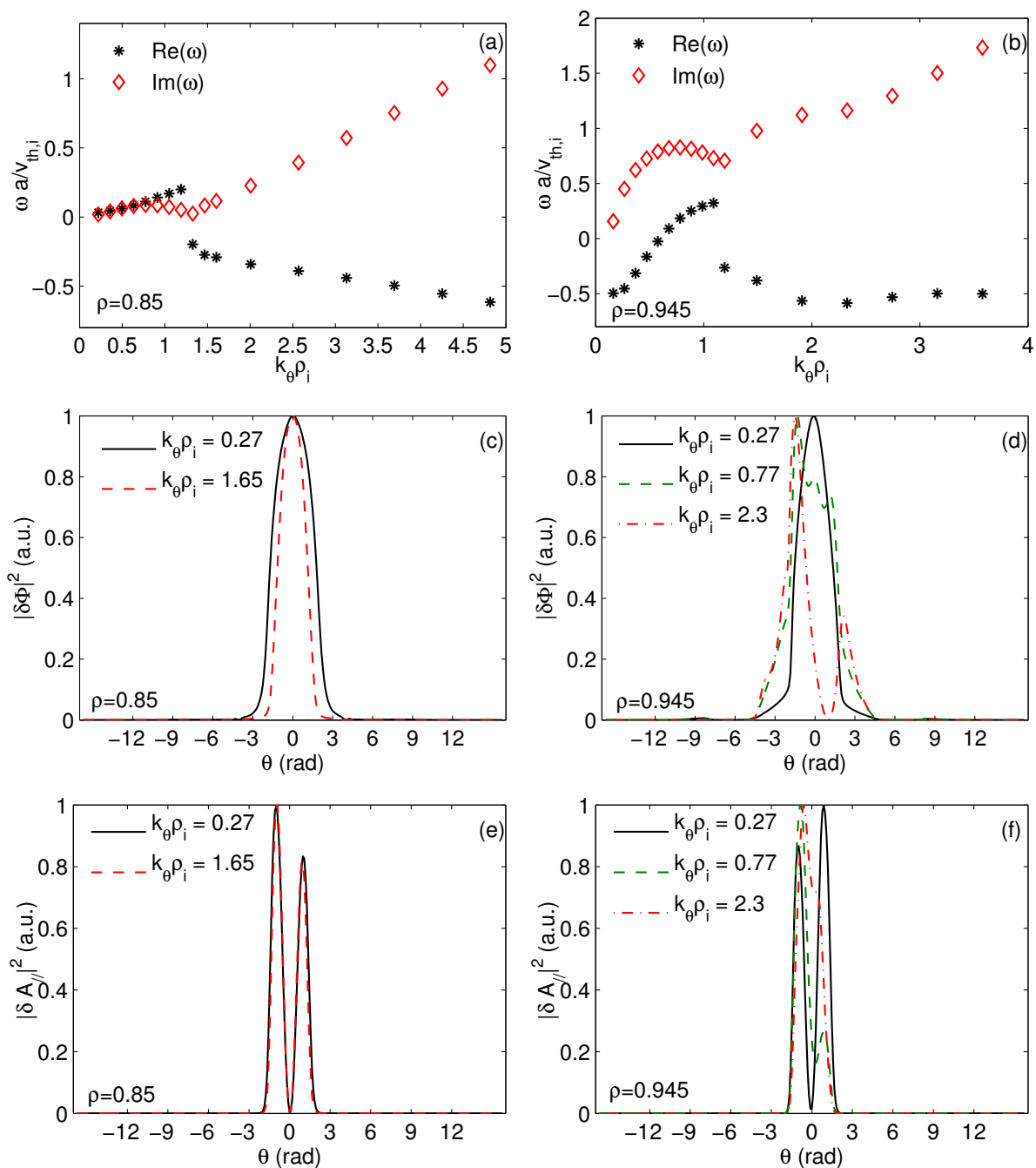


Figure 12.

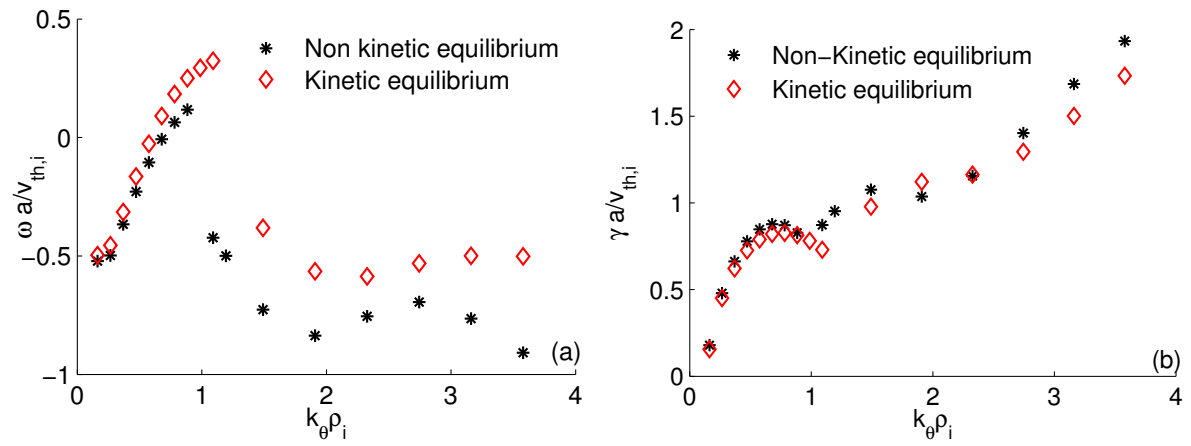


Figure 13.